Journal of Spinal Disorders
Vol. 7, No. 2, pp 102–110

Three-Dimensional Finite Element Modeling of a Cervical Vertebra: An Investigation of Burst Fracture Mechanism

Kevin J. Bozic, *Joyce H. Keyak, *†Harry B. Skinner, †H. Ulrich Bueff, and †David S. Bradford

*School of Medicine and †Department of Orthopaedic Surgery, University of California, San Francisco and *Rehabilitation Research and Development Service, Department of Veterans Affairs Medical Center, San Francisco, California, U.S.A.*

Summary: Finite element modeling was used to study the mechanical behavior of a cervical vertebra under axial compressive loading. A three-dimensional (3-D) finite element (FE) model of a mid-cervical vertebra using inhomogeneous material properties was generated from quantitative computed tomographic (CT) scan data. This model improved upon previous vertebral FE models by using a highly refined mesh to represent the 3-D variation in material properties of vertebral bone. Traumatic loading of the vertebra was simulated by applying an axial compressive displacement through linear spring elements. Bone strength was computed from the CT scan data and compared with predicted stress. Based on the maximum shear stress theory of failure, the model predicts initiation of failure in the central cancellous region of the vertebral body. The type of fracture pattern predicted by the model is consistent with the typical cervical burst fracture that is seen clinically after compressive loading of the cervical spine. As such, we have developed a tool that can be useful for validating proposed fracture mechanisms in the cervical spine. **Key Words:** Biomechanics—Burst fractures—Cervical spine—Finite element modeling—Computed tomography.

Cervical spine fractures are among the most serious orthopedic injuries and often have devastating effects on the individual's quality of life. In particular, burst fractures are associated with a high risk of quadriparesis (34). Axial loading has long been considered to be the mechanism of burst fractures (17,21), and experimental data have supported this conclusion (4,17,18,24,28,35,37–41). Furthermore, the bony pattern of vertebral injury has been well described (4,5,35,37), and is often associated with bone fragments in the canal and varying degrees of neurologic deficit.

Evaluation of the mechanism of injury is important in the complete understanding and treatment of spine trauma. Knowledge of the injury mechanism can be helpful in choosing the technique of reduction and management of certain injuries. Many approaches have been used to study injury mechanism in the spine, including clinical observations (2,4,11,35,37), in vivo and in vitro laboratory experimental studies (4,17,22,24,28,30,35,37–41), and, more recently, analytical modeling techniques such as finite element modeling.

In order to obtain clinically valid results, analytical models must represent the complex geometry and material property variations of the bone, and must incorporate realistic loading conditions. Three-dimensional (3-D) finite element (FE) modeling using a highly refined mesh and inhomogeneous material properties can do this and allows detailed evaluation of the internal stress field in bone. Use of FE modeling also permits model parameters to be easily modified

Address correspondence and reprint requests to Dr. Harry B. Skinner, Department of Orthopaedic Surgery, Box 0728, University of California, San Francisco, CA 94143-0728, U.S.A.

This work was presented in part at the 12th annual Southern Biomedical Engineering Conference, Tulane University, New Orleans, LA, April 2–4, 1993.

for comparative studies (33). FE models have been used extensively in the area of spine biomechanics (1,6–10,13,14,21,23,25,28–32), particularly in the thoracolumbar spine. Although many investigators have used FE models to analyze the stresses and deformations in the intervertebral disk (1,6,13,31–33), the facet joints (25,29,31), the end-plate (32,33), and the vertebral body (7–10,14,21,23,28,32,33), only a few studies have dealt with the cervical spine (1,14,25). Furthermore, most of the previous studies using FE techniques to analyze the stresses in vertebral bone are limited by their simplifying assumptions regarding geometric and material properties. Suwito et al. (33) demonstrated that the results of vertebral FE models are sensitive to variations in geometric and material properties, particularly in the assignment of Young's moduli to the elements representing cancellous bone. Many models (8–10,14,21,23,28,32,33) use homogeneous material properties to represent vertebral bone or assign only two moduli—one for cortical and one for cancellous bone. This method fails to realistically represent actual structure.

Other factors that limit the validity of previous FE models of the spine include the assumption of idealized geometry and/or the use of two-dimensional (2-D) analyses (7,13,14,23,25,28,32,33). For instance, studies that use axial symmetry assume that the loading conditions, stress distribution, and material properties will be axisymmetric, and these assumptions limit the ability of these models to represent realistic clinical situations. Furthermore, 2-D models are inadequate for representing the bone geometry and inhomogeneity and for analyzing the complex loading conditions that have been proposed to cause injury in the cervical spine (4,5,11,35,37).

Although previous analytical modeling has contributed to the understanding of the loading, deformation, and stress state of the spine, it is apparent that a more sophisticated, representative method is necessary to realistically evaluate mechanism of injury. We have developed an FE model that can represent the complex geometry and nonhomogeneous material properties of vertebral bone and can be used for investigating cervical vertebral body stresses. The primary goal of the present study is to use this model to illustrate the effects of axial compressive loading on a cervical vertebral body.

METHODS

Model Generation

A 3-D FE mesh was constructed from quantitative computed tomography (QCT) data using the automated method described by Keyak et al. (12). The geometry and material properties of the model were derived from the cervical spine of a 66-year-old man. The specimen was obtained at autopsy and was free of any disk or bony abnormalities. Fifteen contiguous axial CT scan slices (Fig. 1) were obtained using a General Electric 9800 Research Scanner operating at the following settings: 140 kVp; 70 mA; 3 s; slice thickness, 1.5 mm; pixel size, 1.06 mm; 320 × 320 matrix. The slices ranged from the superior surface of C5 to the inferior surface of C3 so as to include all of C4, the vertebra that was modeled. The specimen was scanned in a water-filled cylinder to minimize beam hardening effects and was placed on a Cann-Genant phantom for calibration purposes, as described previously (12). The CT scan data were transferred to a Sun SPARCstation 1 (Sun Microsystems, Mountain View, CA) for model generation and FE analysis.

Model generation proceeded according to the automated method described previously (12). The 3-D geometry of the vertebra was determined using a contour detection algorithm to identify continuous closed contours of the bone surface from each of the CT scan images (26). Elements were generated to represent the bone within these contours. The Young's modulus of each element was derived by first computing the apparent density for each pixel within the element using a linear calibration of the CT scan data (12). The elastic modulus for each pixel was computed from the apparent density using the following empirical equation developed by Carter and Hayes (3):

$$E = 3790\ \dot{\epsilon}^{0.06}\rho^{3} \qquad (1)$$

for $0.001 \le \dot{\epsilon} \le 10.0\ s^{-1}$, $0.10 \le \rho \le 2.0\ g\ cm^{-3}$, where E is the elastic modulus (MPa), $\dot{\epsilon}$ is the strain rate (s^{-1}, assumed to be $0.01\ s^{-1}$ for the entire bone) (15), and ρ is the apparent density ($g\ cm^{-3}$). The modulus for each element was then calculated by averaging the elastic moduli for all of the pixels lying partially or totally within the element. To account for partial volume effects, the modulus for each pixel was scaled according to its volume fraction within the element.

By calculating the modulus independently for each element, this model accounted for the 3-D variation in material properties of the bone. The calculated moduli were rounded to obtain 83 moduli with the following values: 0.01 MPa; $10.5 \times (1.1)^{n-2}$ MPa, n = 2, 3, . . . 83. Poisson's ratio was assumed to be 0.4 (36). The resulting 3-D FE model consisted of 11,726 nodes and 8,590 eight-noded isoparametric cube elements measuring 1.25 mm on a side (Fig. 2).

For failure analysis, the compressive strength of

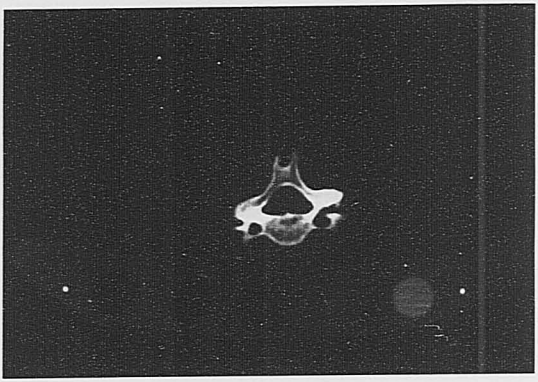

FIG. 1. CT scan image of the mid-cervical vertebra used in this study. The Cann-Genant calibration phantom is shown below the specimen container.

each element was estimated using the empirical equation developed by Carter and Hayes (3) that describes the relationship between strength and apparent density:

$$S_c = 68\ \dot{\epsilon}^{0.06}\rho^2 \qquad (2)$$

for $0.001 \leq \dot{\epsilon} \leq 10.0\ s^{-1}$, $0.10 \leq \rho \leq 2.0\ g\ cm^{-3}$, where S_c is the compressive strength (MPa). The strain rate again was assumed to be $0.01\ s^{-1}$ for the entire bone.

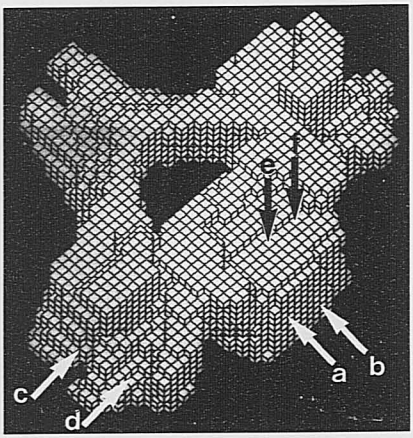

FIG. 2. Superior view of the 3-D FE model (11,726 nodes, 8,590 elements). Arrows refer to planes depicted in Figs. 4–6.

The compressive strength at each node was computed by averaging the strengths of each element that contained that node.

Boundary Conditions

To model the traumatic loading conditions proposed to cause burst fractures in the cervical spine (4,5,37), a uniform compressive axial displacement (4 mm) was applied through 221 linear spring elements added to the superior vertebral body surface (Fig. 3) such that the applied force (determined from the analysis) was 3,400 N. This force represents the average compressive breaking load of a cervical vertebral

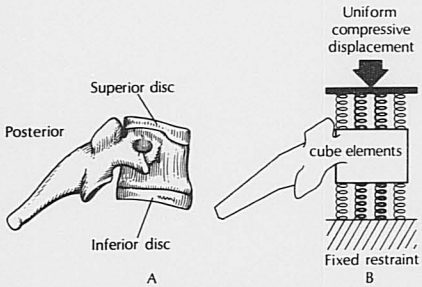

FIG. 3. A: Mid-cervical vertebra with superior and inferior intervertebral disks. **B:** Schematic representation of the condition simulated by the FE model. Uniform compressive displacement was applied to the FE model through linear spring elements. Bold springs represent nucleus (greater stiffness); thin springs represent annulus (lower stiffness).

body (37). Restraint in the inferosuperior direction was provided by 241 linear spring elements connected to the inferior vertebral body surface. The total stiffness of the springs on each surface approximated the stiffness of a cervical intervertebral disk (0.5 MN/m) (19). The total stiffness of the springs covering the central 50% of the surface of the vertebral body (corresponding to the location of the nucleus pulposus) was assumed to be four times the total stiffness of the peripherally located springs (corresponding to the location of the annulus fibrosus) (19,37). This type of stiffness distribution has been suggested by previous investigators who studied the compressive pressure distribution transferred from the intervertebral disk to the vertebral body under external compression (20,21). The stiffness of each spring was determined by dividing the total stiffness of the region (nucleus or annulus) by the total number of springs representing the region so that the stiffness of each spring in that region was the same. Loading by uniform compressive displacement through springs rather than by uniform compressive forces allowed for varying load application across the surface of the vertebral body, thus simulating physiologic conditions more closely (Fig. 3).

Due to the nature of FE analysis, some restraint was required in the mediolateral and anteroposterior directions. This restraint was provided by using springs of very low stiffness (60 N/m), which were attached between the inferior surface of the model and ground. FE analysis showed that almost no load was carried by these springs.

Analysis of Data

The model was analyzed using ABAQUS software (Hibbitt, Karlsson, & Sorensen Inc. Providence, RI), and the average stresses at each node were obtained. For interpretation of the results, the maximum normal stresses (not principal stresses) acting in each of the sagittal, coronal, and axial planes were calculated and plotted using in-house software. The resulting plots illustrated the stress state at each node in the plane of the figure with line length proportional to the stress magnitude and line orientation showing the direction of the stress. For failure analysis, the principal stresses and maximum shear stress at each node were computed. Based on the maximum shear stress theory of failure, the factor of safety at each node was computed by dividing the shear strength at the node (assumed to be half the calculated compressive strength, S_c) by the maximum shear stress at the node (27). The maximum shear stresses and factors of safety at the nodes were plotted using a grey scale. Areas of probable failure (lowest factor of safety) were identified from these data.

RESULTS

Stress

The maximum normal stresses acting in axial, coronal, and sagittal planes are shown in Fig. 4. These stresses are not principal stresses due to the 3-D nature of the stress field. The coronal and sagittal plots demonstrate high compressive stress (0.5–1.0 MPa) through the centrum of the vertebral body (Fig. 4B and C). The axial plots indicate low compressive normal stress acting within the transverse plane, except for a band of compressive stress ~0.5 MPa in magnitude oriented bilaterally from the centrum of the vertebral body toward the pedicles (Fig. 4A).

Grey scale plots of maximum shear stress show peak stresses in the anterior portion of the vertebral body, through the midline of the body, and bilaterally along oblique lines (Fig. 5). Maximum shear stresses in these regions range from 0.5 to 0.8 MPa.

Factor of Safety

Factor of safety plots in the axial plane (Fig. 6A and B) resemble the plots of maximum shear stress. The regions of lowest factor of safety are in the anterior portion of the vertebral body and along the oblique and mid-sagittal lines. Here, the factors of safety range from 0.25 to 1.3. Plots in the coronal plane through the posterior portion of the body (Fig. 6C) show regions of low factor of safety (0.3–1.0) in the center of the vertebral body and inferolaterally near the pedicles (0.2–0.66). The plot ~6 mm anterior to this coronal section (Fig. 6D) shows a different distribution of factor of safety. In this more anterior section, the low factors of safety are located only in the central region of the vertebral body. Sagittal plots (Fig. 6E and F) indicate that low factors of safety (0.25–0.40) are predicted in the central cancellous region of the vertebral body.

DISCUSSION

Analysis of the Cervical Vertebral Body Under Axial Compression

The model predicts high compressive stresses acting in the axial plane along oblique lines from the centrum of the vertebral body to the pedicles (Fig.

4A). This stress field most likely arises due to the restraining effect of the posterior elements on the transverse expansion of the vertebral body. High shear stresses and low factors of safety (using the maximum shear stress failure theory) are also predicted in these

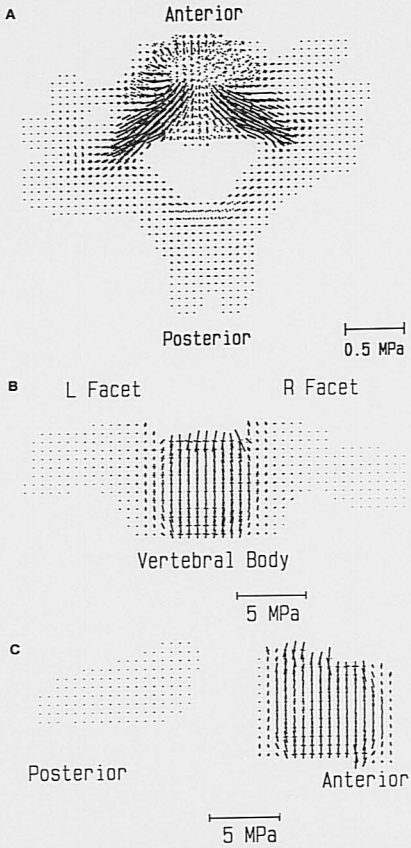

FIG. 4. Maximum normal stresses (not principal stresses) predicted by the FE model at each node in the axial, coronal, and sagittal planes. **A:** The maximum normal stresses in the axial plane passing through point a in Fig. 2. **B:** Stresses in the coronal plane passing through point c in Fig. 2. **C:** Stresses in the midsagittal plane passing through point e in Fig. 2. The midpoint of each line coincides with the location of the stress. Line length is proportional to stress magnitude, and line orientation indicates the direction of the stress. Solid lines represent compression; dotted lines indicate tension.

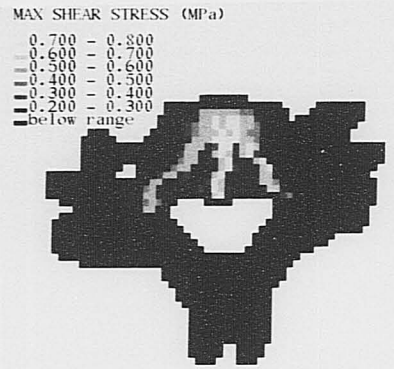

FIG. 5. Maximum shear stresses predicted in the axial plane passing through point a in Fig. 2.

regions (Figs. 5 and 6). When the factor of safety decreases to <1, failure of the bone is predicted to begin. The lowest factor of safety computed with this model is 0.2, indicating that failure would actually begin at a load significantly lower than the 3,400-N load applied in this model. However, computing the factor of safety involves many assumptions regarding material properties and failure theories. Thus, the actual failure load cannot be accurately predicted from this study.

The central cancellous bone of the vertebral body is computed to have the lowest factor of safety, indicating fracture initiation in this region. The precise pattern of fracture propagation cannot be determined rigorously from the current model; however, once failure begins, it is reasonable to expect that fracture propagation will continue from regions of failure to nearby regions of low factor of safety. In this process, the initial failure of the bone would tend to increase the compression, and therefore the stress, on the adjacent intact portions of the vertebral body. This increasing stress would result in decreasing factor of safety in the areas of already low factor of safety, resulting in propagation along the oblique and sagittal lines (Fig. 6A and B). In order to confirm this assumption, an iterative analysis must be undertaken.

Comparison with Previous FE Models

Although many investigators have used FE modeling to evaluate the stress field in the thoracolumbar

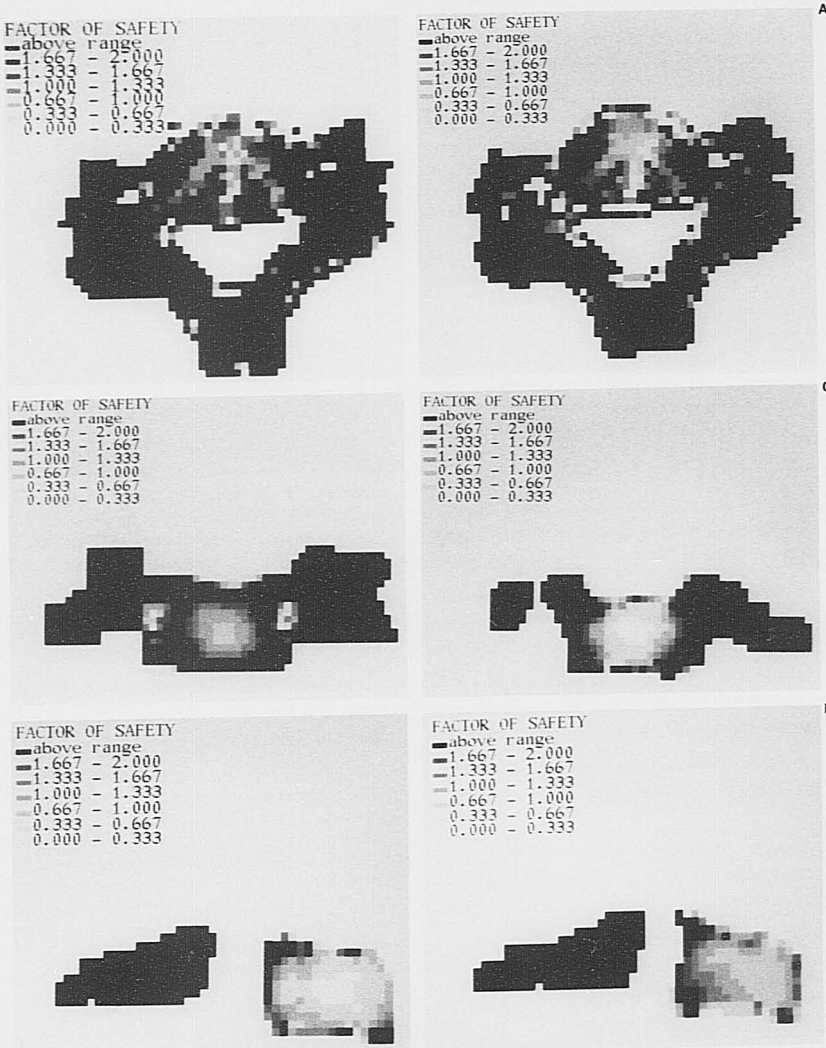

FIG. 6. Factor of safety in the axial **(A and B)**, coronal **(C and D)**, and sagittal **(E and F)** planes. Sections are indicated in Fig. 2.

spine (6–10,13,23,28–33), few have studied the stresses within the vertebral body of the cervical spine (14,25). Kurosawa et al. (14) and Saito et al. (25) used FE modeling to examine the stresses in the cervical spine. However, because the intent of both of these studies was to evaluate deformations of the entire cervical spine, their models used a very course mesh and homogeneous material properties to represent vertebral bone. These types of models are inadequate for providing a detailed examination of the stress field in the vertebral body.

Oxland and Onat (21) used a nonlinear axisymmetric FE model of a thoracic vertebra to investigate the mechanism of thoracolumbar burst fractures. Of note, the results of this model predict early failure in the cancellous bone of the vertebral centrum, consistent with the results of the present model. Also, the nonlinear analysis enabled modeling of the fracture propagation. However, the use of homogeneous material properties to represent cortical and cancellous bone, as well as the assumption of axial symmetry, limit the ability of this model to predict the true, 3-D, nonsymmetric stress distribution within the vertebral body.

Faulkner et al. developed a patient-specific technique for creating 3-D, nonlinear FE models of lumbar vertebral bodies from QCT data to estimate the risk of osteoporotic fractures in the lumbar spine (7). Their use of QCT data enabled realistic representation of the 3-D variation in material properties of vertebral bone and was similar to the technique used in the present study. However, the omission of the posterior elements precluded the model from predicting the oblique stress pattern that was found in the present study.

Our model differs significantly from those of previous studies by using a highly refined mesh to represent the complex geometry and 3-D variation in material properties of vertebral bone. Unlike previous models in which a uniformly distributed load was applied to the vertebra (7,21), the present model used a uniform compressive displacement applied through linear spring elements. This boundary condition resulted in varying stresses along the superior and inferior surface of the vertebral body, suggesting that application of a uniform compressive displacement through spring elements is more realistic than is the application of a uniform compressive load, as suggested by previous investigators (7,21). Our results also demonstrate the 3-D nature of the stress field in the vertebra after axial compressive loading. This result supports the conclusion that the realistic geometry of our model enabled prediction of a fracture pattern that would not have been apparent from a 2-D or axisymmetric model with (or without) homogeneous material properties. Finally, any model that omits the posterior elements would not be able to predict the oblique stress field that arises in our model because of the restraining effect of the posterior elements. As such, we have developed a tool that can be useful for validating proposed injury mechanisms in the cervical spine, as well as for examining the effects of varying boundary conditions on bone stress.

FIG. 7. Axial CT scan of a cervical burst fracture.

Clinical Implications and Limitations

Cervical burst fractures are thought to occur as a result of a traumatic event that subjects the cervical spine to an axial compressive load, such as the one simulated by the present model (4,5,37). The current model predicts that during axial compressive loading of the cervical spine, failure of the vertebral body will begin in the central cancellous area of the vertebral body, a finding consistent with the mechanism of burst fractures in the thoracolumbar spine described previously (21). Furthermore, the regions of low factor of safety that are predicted by this model coincide with the fracture lines that are seen clinically in a typical burst fracture (Fig. 7). This type of fracture pattern may produce the characteristic vertebral body fragments that are associated with burst fractures and can cause neurologic sequelae after retropulsion into the spinal canal.

Although the current study is useful in predicting the stress/strain state in vertebral bone, certain simpli-

fying assumptions were made. The analysis does not consider the strain-rate sensitivity of bone. However, as indicated by Eqs. 1 and 2, the effect of strain rate on bone modulus and strength is minimal (3). Even if the loading rate had been s^{-1}, the elastic moduli would have been only 32% greater. Furthermore, the strength values for each element would have been proportionately higher as well. The failure criteria that were used to predict fracture were based on factor of safety (which involves a ratio of strength to stress). As a result, the effect of strain rate becomes even less significant because the same constant strain rate is used in defining both the elastic modulus and the strength of each element.

Another limiting assumption is that the FE model used in this analysis does not account for the nonlinear material properties of bone, even though it is generally thought that bone behaves as a nonlinear material. Even so, this assumption does not affect the ability of the model to predict failure based on areas of low *relative* factor of safety. Also, in actual traumatic loading, a cervical vertebra is rarely subjected to a purely axial compressive force. Even if axial compression is the major injuring vector (37), other forces due to shear, flexion, extension, lateral bending, and torsion are likely to be present as well. Due to the nonaxisymmetric nature of the current model, future applications could incorporate more complex loading conditions. Finally, the selection of failure criteria for bone is a controversial subject. Many failure theories for bone have been suggested by previous investigators, including the von Mises yield criterion, maximum shear stress theory, Hoffman yield criterion (16), and others. However, development of a more sophisticated failure theory for bone remains to be accomplished, so that the maximum shear stress theory of failure was believed to be adequate for the purposes of this study. In order to validate the results of the current model, in vitro mechanical testing of the human cervical spine must be performed.

Despite the limitations described above, the current model has many potential clinical applications. As described above, we have elucidated the mechanism of cervical burst fractures through FE modeling. In the future, this type of model could be used to examine the mechanism of cervical spine injury under other loading configurations, including flexion, hyperextension, torsion, and lateral bending. The ability to accurately predict fracture patterns could improve the radiologic evaluation and clinical management of patients with cervical spine injury. This model could also be used to evaluate the effect of various boundary conditions, such as those representing cervical fusion or degenerative disk disease, on the stress distribution within an intact vertebra.

Acknowledgment: This research was supported by the Department of Veterans Affairs, Rehabilitation Research and Development Service, and the Department of Orthopaedic Surgery, University of California, San Francisco. We thank Irving Lee, B.S.M.E., and Jeffrey Lotz, Ph.D., for their insightful comments.

REFERENCES

1. Belytschko T, Kulak RF, Schultz AB, Galante JO: Finite element stress analysis of an intervertebral disc. *J Biomech* 7:277–285, 1974
2. Bohlmann HH: Acute fractures and dislocations of the cervical spine: an analysis of 300 hospitalized patients and review of the literature. *J Bone Joint Surg [Am]* 61:119–142, 1979
3. Carter DR, Hayes WC: The compressive behavior of bone as a two-phase porous structure. *J Bone Joint Surg [Am]* 59:954–962, 1977
4. Cervical Spine Research Society Editorial Committee. *The Cervical Spine*, 2nd ed, Philadelphia, PA, JB Lippincott, 1989
5. Clark CR, Igram CM, el-Khoury GY, Ehara S: Radiographic evaluation of cervical spine injuries. *Spine* 13:742–747, 1988
6. Duncan NA, Ahmed AM: The role of axial rotation in the etiology of unilateral disc prolapse: an experimental and finite-element analysis. *Spine* 16:1089–1098, 1991
7. Faulkner KG, Cann CE, Hasegawa BH: Effect of bone distribution of vertebral strength: assessment with patient-specific nonlinear finite element analysis. *Radiology* 179:669–674, 1991
8. Hakim NS, King AI: An experimentally validated three-dimensional finite element model of a vertebra. In: *Advances in Bioengineering* New York, ASME, pp. 11–12, 1976
9. Hakim NS, King AI: A computer aided technique for the generation of a 3-D finite element model of a vertebra. *Comput Biol Med* 8:187–196, 1978
10. Hakim NS, King AI: A three-dimensional finite element dynamic response analysis of a vertebra with experimental verification. *J Biomech* 12:277–292, 1979
11. Huelke DF, Nusholtz GS: Cervical spine biomechanics: a review of the literature. *J Orthop Res* 4:232–245, 1986
12. Keyak JH, Meagher JM, Skinner HB, Mote CD Jr: Automated three-dimensional finite element modelling of bone: a new method. *J Biomed Eng* 12:389–397, 1990
13. Kim YE, Goel VK, Weinstein JN, Lim TH: Effect of disc degeneration at one level on the adjacent level in axial mode. *Spine* 16:331–335, 1991
14. Kurosawa H, Yamanoi T, Yamakoshi K: Radiographic findings of degeneration in cervical spines of middle-aged soccer players. *Skeletal Radiol* 20:437–440, 1991
15. Lanyon LE, Hampson WGJ, Goodship AE, Shah JS: Bone deformation recorded *in vivo* from strain gauges attached to the human tibial shaft. *Acta Orthop Scand* 46:256–268, 1975
16. Lotz JC, Cheal EJ, Hayes WC: Fracture prediction for the proximal femur using finite element modeling, part I: linear analysis. *J Biomech Eng* 113:353–360, 1991
17. McElhaney JH: Biomechanical aspects of neck injury. Biomedical Engineering Department, Duke University, 1979
18. McElhaney JH, Paver JG, McCracklin HJ: Cervical spine compression responses. In: Proceedings of the 27th STAPP Car Crash Conference, San Diego, CA, 1983. Warrendale, PA, Society of Automotive Engineers, 1983, p 163
19. Moroney SP, Schultz AB, Miller JA, Andersson GB: Load-displacement properties of lower cervical spine motion segments. *J Biomech* 21:769–779, 1988

20. Nachemson AL, Morris JM: *In vivo* measurements of intradiscal pressure. *J Bone Joint Surg* 46:1077, 1964
21. Oxland TR, Onat ET: Thoracolumbar burst fracture mechanism: the effect of disc degeneration using a non-linear finite element analysis. In: Transactions of the 39th Annual Meeting of the Orthopaedic Research Society, San Francisco, CA, February 15–18, 1993
22. Panjabi MM, Summers DJ, Pelker RR, Videman T, Friedlaender GE, Southwick WO: Three-dimensional load-displacement curves due to forces on the cervical spine. *J Orthop Res* 4:152–161, 1986
23. Ranu HS: A vertebral finite element model and its response to loading. *Med Prog Technol* 16:189–199, 1990
24. Roaf R: A study of the mechanics of spinal injury. *J Bone Joint Surg* [*Br*] 42:810–818, 1960
25. Saito T, Yamamuro T, Shikata J, Oka M, Tsutsumi S: Analysis and prevention of spinal column deformity following cervical laminectomy. I: pathogenetic analysis of postlaminectomy deformities. *Spine* 16:494–502, 1991
26. Seitz P, Ruegsegger P: Fast contour detection algorithm for high precision quantitative CT. *IEEE Trans Med Imaging* 2:136–141, 1983
27. Shigley JE: *Mechanical Engineering Design*, 3rd ed, New York, McGraw-Hill, 1977
28. Shirado S, Kaneda K, Tadano S, Ishikawa H, McAfee PC, Warden KE: Influence of disc degeneration on mechanism of thoracolumbar burst fractures. *Spine* 17:286–292, 1992
29. Shirazi-Adl SA: Finite-element evaluation of contact loads on facets of an L2-L3 lumbar segment in complex loads. *Spine* 16:533–541, 1991
30. Shirazi-Adl SA: Dynamics of human lumbar intervertebral joints: experimental and finite-element investigations. *Spine* 17:93–102, 1992
31. Shirazi-Adl SA: Finite-element simulation of changes in the fluid content of human lumbar discs: mechanical and clinical implications. *Spine* 17:206–212, 1992
32. Shirazi-Adl SA, Shrivastava SC, Ahmed AM: Stress analysis of the lumbar disc-body unit in compression: a three-dimensional nonlinear finite element study. *Spine* 9:120–134, 1984
33. Suwito W, Keller TS, Basu PK, Weisberger AM, Strauss AM, Spengler DM: Geometric and material property study of the human lumbar spine using the finite element method. *J Spinal Disord* 5:50–59, 1992
34. Torg JS: Epidemiology, pathomechanics, and prevention of athletic injuries to the cervical spine. *Med Sci Sports Exerc* 17:295–303, 1985
35. Torg JS, Pavlov H, O'Neill MJ, Nichols CE Jr, Sennett B: The axial load teardrop fracture: a biomechanical, clinical, and roentgenographic analysis. *Am J Sports Med* 19:355–364, 1991
36. Van Buskirk WC, Ashman RB: The elastic moduli of bone. *Trans ASME* 45:131–143, 1981
37. White AA, Panjabi MM: *Clinical Biomechanics of the Spine*, 2nd ed, Philadelphia, PA, JB Lippincott, 1990
38. Yoganandan N, Pintar FA, Sances A Jr, Reinartz J, Larson SJ: Strength and kinematic responses of dynamic cervical spine injuries. *Spine* 16S:511–517, 1991
39. Yoganandan N, Sances A Jr, Maiman DJ, Myklebust JB, Pech P, Larson SJ: Experimental spinal injuries with vertical impact. *Spine* 11:855–860, 1986
40. Yoganandan N, Sances A Jr, Pintar F: Biomechanical evaluation of the axial compressive responses of the human cadaveric and manikin necks. *J Biomech Eng* 111:250–255, 1989
41. Yoganandan N, Sances A Jr, Pintar F, Maiman DJ, Reinartz J, Cusick JF: Injury biomechanics of the human cervical column. *Spine* 15:1031–1039, 1990